ISSN 0023-1584, Kinetics and Catalysis, 2012, Vol. 53, No. 2, pp. 253–261. © Pleiades Publishing, Ltd., 2012.
Original Russian Text © A.E. Yarulin, R.M. Crespo-Quesada, E.V. Egorova, L.L. Kiwi-Minsker, 2012, published in Kinetika i Kataliz, 2012, Vol. 53, No. 2, pp. 263–271.

Structure Sensitivity of Selective Acetylene Hydrogenation over the Catalysts with Shape-Controlled Palladium Nanoparticles

A. E. Yarulin[a, b], R. M. Crespo-Quesada[a], E. V. Egorova[b], and L. L. Kiwi-Minsker[a]

[a] *Group of Catalytic Reaction Engineering, Ecole Polytechnique Fédérale de Lausanne, Switzerland*

[b] *Moscow State Academy of Fine Chemical Technology, Moscow, 117571 Russia*

e-mail: lioubov.kiwi-minsker@epfl.ch

Received May 27, 2011

Abstract—The structure sensitivity of acetylene hydrogenation on catalysts with controlled shape of palladium nanoparticles was studied. Palladium particles of cubic (Pd_{cub}), cuboctahedral (Pd_{co}) and octahedral (Pd_{oct}) shapes were obtained by a colloidal method. Poly(*N*-vinyl)pyrrolidone (PVP) was used as the stabilizer of colloidal solutions. In order to eliminate the effect of the polymer on the properties of the catalyst, PVP was removed from the surface of the particles after their transfer to the support by simultaneous treatment with ozone and UV radiation. This allowed complete cleaning of the catalyst surface from the organic stabilizer without any change in the morphology of particles. The effectiveness of this treatment method was confirmed by X-ray photoelectron spectroscopy and scanning electron microscopy. It was found experimentally that the shape of nanoparticles does not influence the catalyst selectivity, but the activity decreases in the order $Pd_{oct} > Pd_{co} > Pd_{cub}$. Since octahedrons consist of (111) faces, the cubes contain only (100) faces, and the cuboctahedrons are composed of faces of both types, Pd_{111} is more active than Pd_{100}. Calculations with the use of a statistical method showed that the ~3-nm Pd octahedrons are nanoparticles with optimum shape and size, giving maximum catalyst activity.

DOI: 10.1134/S0023158412020152

INTRODUCTION

Selective acetylene hydrogenation is used in industry to remove C_2H_2, which poisons the catalyst for the polymerization of ethylene, from gas mixtures. In order to avoid poisoning, the acetylene content should not exceed 5 ppm [1].

Catalysts based on palladium nanoparticles ensure the hydrogenation of acetylene with high selectivity [1–3]. Nevertheless, the oligomers of acetylene (so-called green oil) and also ethane can be formed as reaction by-products.

The activity and selectivity of a catalyst can depend on the size [4, 5] and shape [6, 7] of its particles. It was shown that the reaction of acetylene hydrogenation has antipathetic structure sensitivity [4, 8, 9]; i.e., the catalyst turnover frequency (TOF) increases with particle size. It is worth noting that, the fraction of atoms located on the faces also increases with size (in comparison with the fractions of atoms at the edges and apexes). Consequently, these atoms are the most active in this reaction. The shape of nanoparticles can also influence the properties of the catalyst. The cubic particles are composed of (100) faces, the octahedrons consist of only (111) faces, and the cuboctahedrons contain faces of both of these types. Different faces possess different activities. This circumstance can be used in the optimization of the properties of the catalyst in structure-sensitive reactions.

A lot of works on structure sesitivity were devoted to the study of the influence of particle size on the catalyst activity [8–10], whereas the influence of particle shapes is scantily known. A possible reason is that nanoparticles with controlled shape and size are difficult to synthesize. However, recent advances in the colloidal methods of synthesis solved this problem [11, 12]. The preparation of colloidal solutions of metal nanoparticles allows obtaining the particles of desired morphology. Organic polymer compounds are usually applied to stabilize nanoparticles. However polymers remain on the surface of active sites after their transfer onto the support. Calcination in air [13] and heat treatment in a vacuum [14] or in flowing hydrogen [15] are commonly used to remove the stabilizer. However, severe treatment conditions can affect the morphology of the particles. An alternative method for removal of organic stabilizers is simultaneous treatment with ozone and short-wavelength ultraviolet radiation (UV–O_3) which causes the decomposition of organic molecules to CO_2, H_2O, N_2 [16]. This method was successfully applied to cleaning the surfaces of Pt [17] and Au nanoparticles [18].

In this work, we obtained cubic Pd nanoparticles containing (100) faces, octahedrons consisting of

(111) faces, and cuboctahedrons having both (100) and (111) faces. A method using poly(*N*-vinyl)pyrrolidone (PVP) as the stabilizer was used in the synthesis of nanoparticles with a controlled shape. Carbon nanofibers (CNFs) on sintered metal filters (SMFs) served as the catalyst support. After the deposition of Pd nanoparticles on the support, the samples were treated by the UV–O_3 method in order to remove PVP. The structure sensitivity of selective acetylene hydrogenation was studied on the resulting Pd/CNF/SMF catalysts.

EXPERIMENTAL

Catalyst Preparation

Growth of CNFs on SMFs. The filters of metallic fibers (Inconel alloy or $SMF_{Inconel}$ from Bakaert Fibre Technology, Belgium) were used as a substrate for the growth of CNFs. The alloy Inconel 601 had the following composition, %: Ni, 60.5; Cr, 23; Al, 1.25; Cu, 1.0; Mn, 1.0; Si, 0.5; C, 0.1; S, 0.015; and the balance Fe. The diameter of fibers was 8 μm; the thickness of filters was 0.49 mm, and the porosity was 80%. Before use, the filters were calcined at 650°C for 3 h and were then cut into disks with a diameter of 24 mm.

The growth of CNFs on the Inconel filters ($CNF/SMF_{Inconel}$) was described elsewhere [19, 20]. The chemical vapor deposition of ethane was conducted in the presence of hydrogen in a tubular quartz reactor with an inner diameter of 24 mm. The filters were prereduced in flowing hydrogen (120 mL/min under standard conditions: atmospheric pressure of 10^5 Pa and 25°C) at 625°C for 2 h (heating rate of 10 K/min). The synthesis was performed at 675°C for 1 h. The reaction mixture had the following composition: Ar : C_2H_6 : H_2 = 80 : 3 : 17 (flow rate of 600 mL/min, standard conditions). Then, the reactor was cooled in a flow of a mixture of argon and hydrogen (120 mL/min, standard conditions) to 450°C and, after this, in a flow of argon to room temperature. In the course of the entire process, a pressure of 125 kPa was maintained in the reactor.

Synthesis of palladium nanoparticles and the UV–O_3 treatment. The nanoparticles of palladium with controlled shape and size were synthesized by a colloid method, which was described in detail in [21]. The particles in the shape of cubes (Pd_{cub}), cuboctahedrons (Pd_{co}), and octahedrons (Pd_{oct}) were obtained. The stabilizer (PVP) and reducing agent (ascorbic or citric acid) were diluted with 8 mL of water in a round-bottom flask with a reflux condenser. The mixture was heated in an oil bath to 100°C. For obtaining the octahedral particles, the bath was heated only to 90°C. Next, 3 mL of an aqueous solution of Na_2PdCl_4 was syringed into the flask. In the synthesis of the cubic nanoparticles, KBr was also added. The resulting colloidal solution was maintained at a preset temperature under vigorous stirring for 3 (Pd_{cub} and Pd_{co}) or 26 h (Pd_{oct}). For removal of excess PVP, the reaction mixture was diluted with acetone and centrifuged, and the PVP-covered nanoparticles were redispersed in ethanol.

The nanoparticles were deposited onto the support by incipient wetness impregnation followed by vacuum drying at 50°C. The palladium content of CNF was regulated by changing the number of impregnations.

For removal of PVP from the catalyst surface, UV–O_3 cleaning was used. For this purpose, an 8-W UV lamp (Helios Quartz, Italy), which emitted light at 185 and 257 nm, in a home-made metal housing was used. The sample was secured in a holder, which was placed at a distance of 5 mm from the lamp surface, and both sides of the catalyst were cleaned for 4 h.

Catalyst Characterization Methods

The Pd content of the catalyst was determined by atomic absorption spectrometry with a Shimadzu AA-6650 instrument (Japan) at a wavelength of 475 nm.

The chemical composition of the catalyst surface before and after UV irradiation was determined by X-ray photoelectron spectroscopy (XPS) on a Kratos spectrometer (United Kingdom). The measurements were carried out using monochromatic AlK_α radiation (1486.6 eV). The X-radiation power was 150 W.

The morphology of the catalyst surface was studied by scanning electron microscopy (SEM) on an FEI XL30 SFEG microscope equipped with a thermoluminescence detector.

The size and structure of Pd nanoparticles were determined by transmission electron microscopy (TEM) on a CM20 FEG microscope (Philips). Before performing the analysis, the colloidal solution of performing was supported onto copper gauzes and dried in air with an infrared lamp for at least 1 h.

Acetylene Hydrogenation

Figure 1 shows a schematic representation of the experimental installation and reactor. The reaction was carried out in a metallic tubular reactor with an inner diameter of 12 mm. In order to ensure the catalyst position perpendicular to the gas flow, the Pd/CNF/SMF disk was placed at the center of the reactor between two rings. For uniform flow distribution in the reactor volume and for preheating of the reaction mixture, the upper part of the reactor was filled with glass beads. A pressure of 104 kPa was maintained during the reaction. The concentration of products was determined by HP 6890 gas chromatograph (Agilent Technology AG, Switzerland) with a Carboxen 1010 capillary column (Fluka Holding AG, Switzerland). The reaction conditions were the following: temperature, 353–393 K; the partial pressures of acetylene and hydrogen, $P_{C_2H_2}$ = 1.4–4.2 and P_{H_2} =

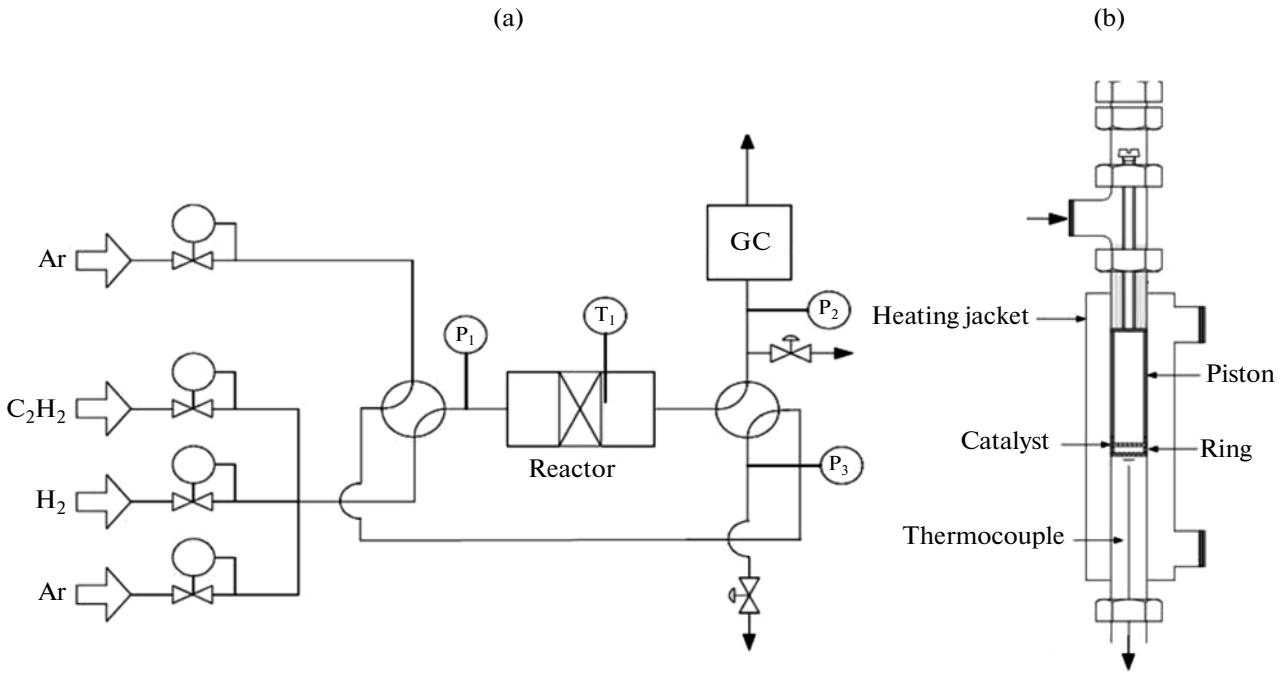

Fig. 1. Schematic diagrams of (a) the installation and (b) the reactor for acetylene hydrogenation.

12–22 kPa, respectively; Ar : C_2H_2 : H_2 = 78.5 : 1.5 : 20; gas flow rate, F = 200–1200 mL/min; acetylene conversion, x = 13%.

Calculation of Reaction Parameters

Conversion and selectivity. The conversion of acetylene was determined from the equation

$$x_{C_2H_2} = \frac{C^0_{C_2H_2} - C^c_{C_2H_2}}{C^0_{C_2H_2}}, \quad (1)$$

where $C^0_{C_2H_2}$ and $C^c_{C_2H_2}$ are the initial and current concentrations of acetylene, respectively.

The acetylene selectivity (S) was calculated as the molar ratio of the concentration of the resulting ethylene ($C_{C_2H_4}$) to the concentration of converted acetylene:

$$S_{C_2H_4} = \frac{C_{C_2H_4}}{C^0_{C_2H_2} - C^к_{C_2H_2}}. \quad (2)$$

The ethane selectivity was estimated in a similar way:

$$S_{C_2H_6} = \frac{C_{C_2H_6}}{C^0_{C_2H_2} - C^c_{C_2H_2}}. \quad (3)$$

Since only C_2H_2, C_2H_4, C_2H_6, and Ar were detected at the reactor outlet, it was assumed that the green oil formed as a result of the oligomerization of acetylene remained on the catalyst surface. Accordingly, the green oil selectivity was calculated as

$$S_{go} = 1 - (S_{C_2H_4} + S_{C_2H_6}). \quad (4)$$

Reaction rate and catalyst turnover frequency. In the course of calculations, the acetylene–catalyst surface contact time (τ'), which depends on the catalyst weight m_{Cat} and the flow rate F, was used instead of the residence time of gas in the reactor (τ):

$$\tau' = \tau\frac{m_{Cat}}{V_F} = \frac{m_{Cat}}{F}, \quad (5)$$

where V_r is the reactor volume.

The experiments were performed in a flow reactor with a thin catalyst bed. At a low conversion (~13%), the ethylene conversion rate is

$$-R_{C_2H_2} = \frac{C^0_{C_2H_2} - C^c_{C_2H_2}}{\tau'}. \quad (6)$$

The turnover frequency of the catalyst was determined from the equation

$$TOF = \frac{-R_{C_2H_2}}{D}, \quad (7)$$

where D is the degree of dispersion of the nanoparticles, i.e., the fraction of atoms arranged on the particle

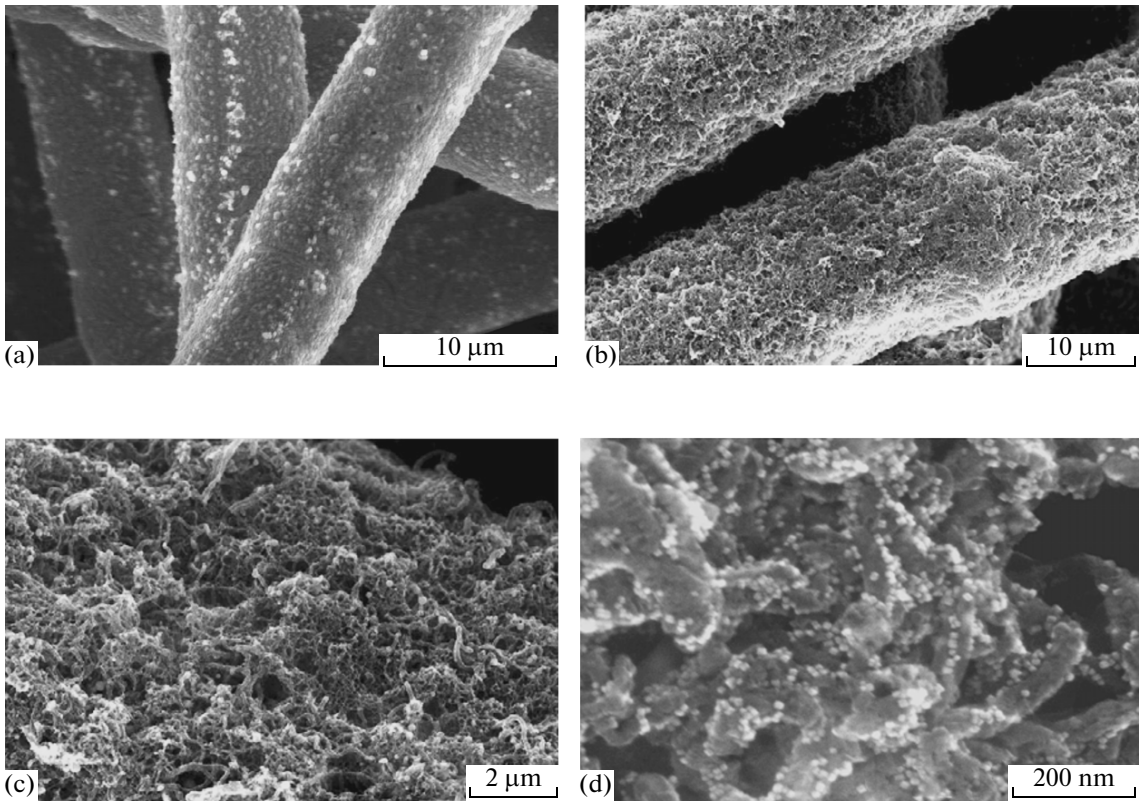

Fig. 2. Micrographs obtained by high-resolution SEM: (a) SMF after calcination, (b) the CNF/SMF support, (c) a magnified image of carbon nanofibers, and (d) Pd_{cub} particles supported on CNF/SMF.

surface, N_s, divided by the total number of atoms in the particle, N_Σ:

$$D = \frac{N_s}{N_\Sigma}. \quad (8)$$

RESULTS AND DISCUSSION

Catalyst Characterization

Morphology. Figure 2 shows the SEM images of the catalyst at different preparation stages. Figure 2a shows a micrograph of the $SMF_{Inconel}$ filter after heat treatment. The filter diameter was ~8 μm. After reduction in a flowing hydrogen and the chemical vapor deposition of ethane, CNFs uniformly covering the SMF fibers were formed (Fig. 2b). The magnified image of the CNFs (Fig. 2c) exhibits a porous structure of the fibers and Ni/Fe particles about 100 nm in size, which served as the catalyst in CNF growth. The nanoparticles of palladium are uniformly distributed over the surface of the support (Fig. 2d).

Figure 3 shows typical micrographs of the palladium nanoparticles obtained by TEM. There are particles of three types. The cubic particles of palladium (Pd_{cub}) contain only (100) faces (Fig. 3a). Their size is 10 nm. The particles of palladium as cuboctahedrons (Pd_{co}) have (100) and (111) faces, and their size is 4.5 nm (Fig. 3b). The third sample (Pd_{oct}) consists of particles as octahedrons, truncated tetrahedrons, and decahedrons containing only (111) faces, and it is characterized by a bimodal particle size distribution.

UV–O_3 treatment. The UV–O_3 treatment was used to remove PVP from the catalyst surface. The process consists in the oxidation of organic matter under the action of ozone and ultraviolet irradiation [17]. Absorbing short-wavelength UV radiation, organic molecules undergo excitation and/or dissociation. Simultaneously, the decomposition of O_2 with the formation of atomic oxygen and ozone occurs under the action of UV light with $\lambda < 245.4$ nm. Atomic oxygen also forms upon the dissociation of ozone under UV radiation. The decomposition products of organic matter—excited molecules and free radicals—interact with atomic oxygen to form simpler volatile molecules, such as CO_2, H_2O, and N_2 [16].

In order to trace the changes in the morphology of nanoparticles in the course of treatment, high-resolution SEM was used. The photographs taken before and after 6-h UV irradiation (they are not given in this article) suggest that the particles retained their shape and size. No particle agglomeration was observed.

The efficiency of the method was evaluated by XPS. The XPS spectra were measured before and after

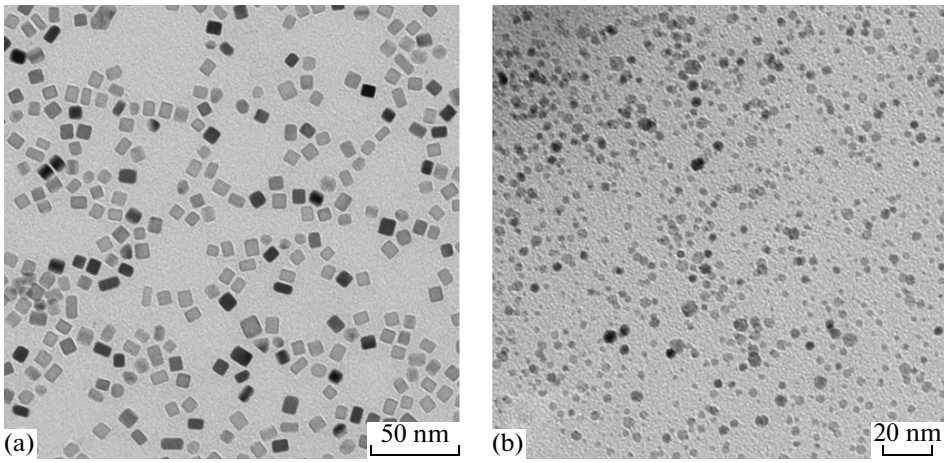

Fig. 3. Typical TEM micrographs of palladium nanoparticles: (a) Pd_{cub} and (b) Pd_{co}.

the UV–O_3 treatment of the samples for 2, 4, and 6 h. The results indicated that about 65% of the PVP was removed from the surface even after treatment for 2 h (a considerable decrease in the intensity of the N 1*s* peak at 400 eV was observed). After 4-h and 6-h treatments, the peak of nitrogen completely disappeared from the spectrum; this fact demonstrates the PVP removal efficiency. The inset in Fig. 4 shows how the fraction of nitrogen changes during surface cleaning relative to its initial content. This method effectively cleaned only the surface oriented toward the UV lamp (curve *1*). Complete cleaning requires sequential 4-h treatment of both sides of the catalyst.

The XPS spectrum of palladium exhibited a doublet of the Pd $3d_{5/2}$ (~335 eV) and Pd $3d_{3/2}$ (~341 eV) peaks. The peaks broadened with treatment time. This can be most clearly seen if we compare the fresh catalyst with the catalyst subjected to 6-h cleaning. The peak broadening is due to the increase in the fraction of $Pd^{\delta+}$, relative to Pd^0, on the catalyst surface. It is likely that the formation of $Pd^{\delta+}$ is caused by the deactivation of palladium as a result of the formation of a surface oxygen layer rather than the oxidations of palladium to PdO. This is evidenced by the fact that the morphology of particles remained unchanged after the UV–O_3 treatment. The oxygen layer can be easily removed with flowing hydrogen during the reaction.

Acetylene Hydrogenation

Structure sensitivity. The reaction scheme of acetylene hydrogenation is given below. In addition to ethylene, ethane can also be formed as a result of either the further hydrogenation of ethylene or the direct hydrogenation of acetylene. The oligomerization of acetylene also yields of green oil.

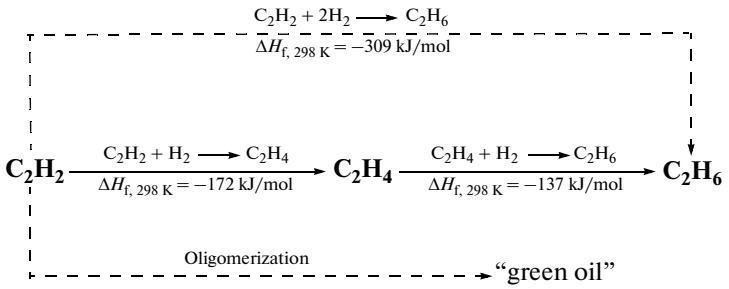

Reaction scheme of acetylene hydrogenation.

The structure sensitivity of the reaction was studied on the Pd/CNF/SMF catalyst with the nanoparticles of Pd_{cub} containing (100) faces, Pd_{oct} with (111) faces, and Pd_{co} with faces of both types. The statistical approach makes it possible to determine the numbers of atoms of each type on the surface of nanoparticles of given shape and size [6]. Thus, it is possible to calculate the fractions of atoms located on the faces, edges, and apexes of the particle. Table 1 summarizes the data for the catalysts used in this work.

To evaluate the catalyst turnover frequency, we used the following computational model:

$$\mathrm{TOF} = x_{111}\mathrm{TOF}_{111} + x_{100}\mathrm{TOF}_{100} + x_{\mathrm{edge}}\mathrm{TOF}_{\mathrm{edge}}. \quad (9)$$

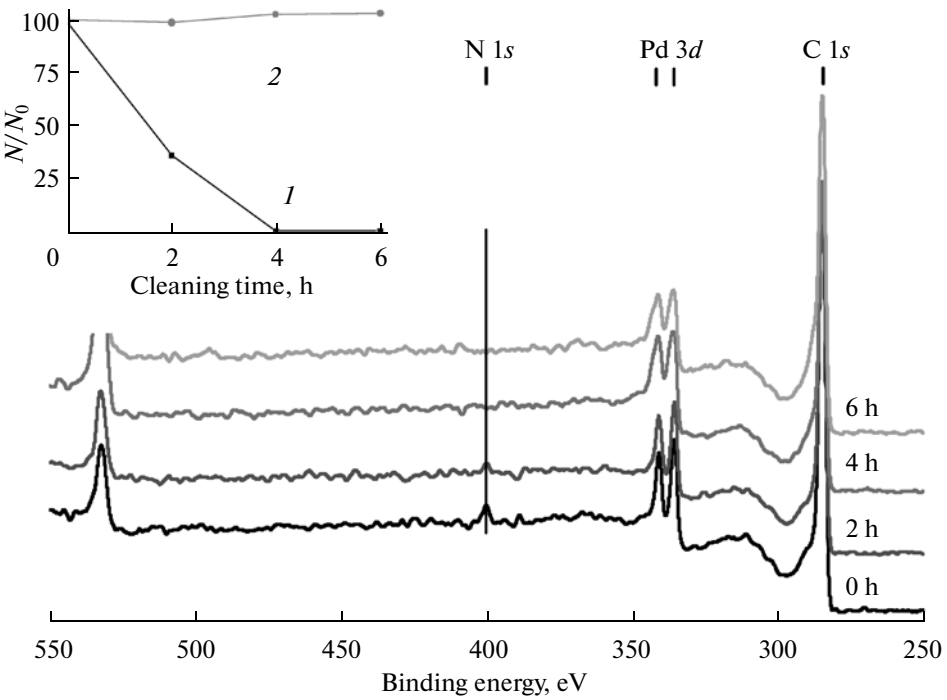

Fig. 4. XPS spectra of Pd_{cub}/CNF/SMF samples before and after cleaning by the UV–O_3 method for 2, 4, and 6 h. Insert: Changes in the nitrogen content of the sample in the course of cleaning (*1*) the surface oriented toward the UV lamp and (*2*) on the opposite side.

This model is based on the assumption that the observed total turnover frequency is a linear function of the fractions of atoms of each type (x_i) and their individual activities (TOF_i). Table 2 summarizes the results of these calculations. As can be seen, the atoms located on the faces of nanoparticles (Pd_{111} and Pd_{100}) exhibited the greatest activity, whereas the activity of low-coordinated atoms on particle edges (TOF_{edge}) was lower by an order of magnitude. This fact confirms the concept of the antipathetic structure sensitivity of the reaction: the fraction of atoms located on the faces of nanoparticles increases with particle size; therefore, the catalyst turnover frequency increases. In turn, Pd_{111} is more active than Pd_{100} by a factor of about 1.5. Consequently, not only the size but also the shape of particles is important. The Pd_{oct} atoms are the most active because these particles contain only (111) faces. Thus, it can be assumed that the hydrogenation of acetylene occurs at the surface atoms of all types, but the catalyst activity depends on the size and shape of the nanoparticles.

Figure 5 shows the dependence of catalyst selectivity and activity on the shape of the particles. The ethylene selectivity is approximately the same on all of the catalysts, and the turnover frequency increases in the order $Pd_{cub} < Pd_{co} < Pd_{oct}$. As was found earlier [3, 22], the selectivity increases with reaction temperature. As the temperature is increased, the desorption of ethylene is facilitated and its hydrogenation to ethane is thus prevented. The selectivity also depends on the ratio between the partial pressures of hydrogen and acetylene. At a relatively low $P_{H_2} : P_{C_2H_2}$ ratio, the polymerization of the latter yields green oil. At a high partial pressure of hydrogen, the nonselective complex β-PdH forms [22, 23], which increases the rate of the hydrogenation of acetylene to ethane. Therefore, an optimum ratio between hydrogen and acetylene should be chosen in order to maximize the yield of ethylene.

Table 1. Statistical data for the surface atoms of Pd_{cub}, Pd_{co}, and Pd_{oct} particles

Catalyst	D, %	Fraction of atoms x_i		
		x_{111}	x_{100}	x_{edge}
Pd_{cub}	10.5	–	0.96	0.04
Pd_{co}	23.5	0.69	0.15	0.16
Pd_{oct}	6	0.97	–	0.03

Table 2. Activity of the surface atoms of Pd_{cub}, Pd_{co}, and Pd_{oct} particles

Catalyst	$-R_{C_2H_2}$, (mol C_2H_2) (mol Pd)$^{-1}$ s^{-1}	Catalyst turnover frequency, s^{-1}			
		TOF	TOF_{111}	TOF_{100}	TOF_{edge}
Pd_{cub}	31.7	301.9	–	313.7	20.0
Pd_{co}	90.0	394.6	497.9	316.9	23.3
Pd_{oct}	28.1	469.1	482.9	–	20.0

Pd_{oct}, which contains only (111) faces, exhibits the highest activity, whereas Pd_{cub}, which consists of only (100) faces, is the least active. The activity of Pd_{co}, whose particles contain faces of both types, has an intermediate value. Hence, we can conclude that, at the same reaction selectivity on (100) and (111) faces, the reaction occurs more rapidly on Pd_{111}; i.e., the activity depends not only on particle size, as found earlier [8, 9], but also on the shape of the particles. This is consistent with the accepted model (Eq. (9)).

The difference in activity can be caused by electronic and geometric factors. The influence of particle size on the activity is explained by the geometric effect, which is due to the dependence of the proportions of surface atoms of different types on the particle size (see Introduction). The essence of the electronic effect is the interactions between the *d* orbitals of the metal and the molecular orbitals of the reactants and reaction products. If the interactions are strong, the strength of substance adsorption on the catalyst surface is significant [23]. It was found that an alkyne is adsorbed on palladium more strongly than an alkene or an alkane [24, 25]. This fact explains the selectivity of palladium catalysts in the hydrogenation of a triple bond. On the other hand, the adsorption of the reactant on the surface should not be so strong as to prevent the reaction from proceeding sufficiently rapidly. Because Pd_{111} is more active than Pd_{100}, it can be assumed that acetylene is more strongly adsorbed on (100) faces; therefore, the reaction occurs on them more slowly than on (111) faces.

Optimization of the size and shape of Pd nanoparticles. The optimization of the size and shape of Pd nanoparticles was based on the accepted model (Eq. (9)) considering activity as the optimization criterion. Since acetylene hydrogenation exhibits antipathetic structure sensitivity, the turnover frequency of the catalyst increases with the size of active particles. On the other hand, the activity based on the total number of particles decreases with the particle size

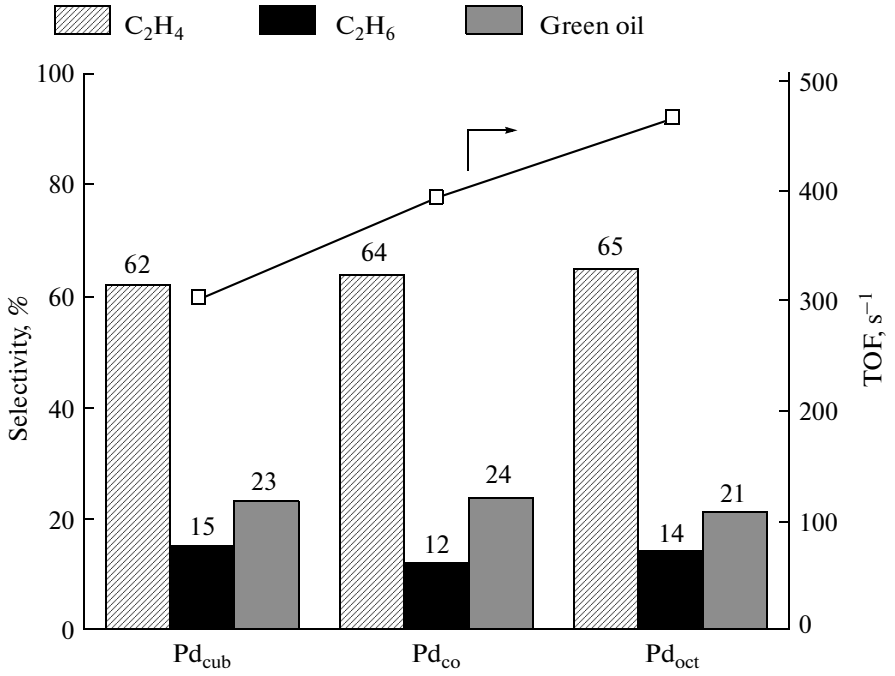

Fig. 5. Catalyst turnover frequency and reaction selectivity on Pd_{cub}, Pd_{co}, and Pd_{oct} particles. Reaction conditions: $P_{C_2H_2}$ = 1.4 kPa; P_{H_2} = 21 kPa; 393 K; x = 13%.

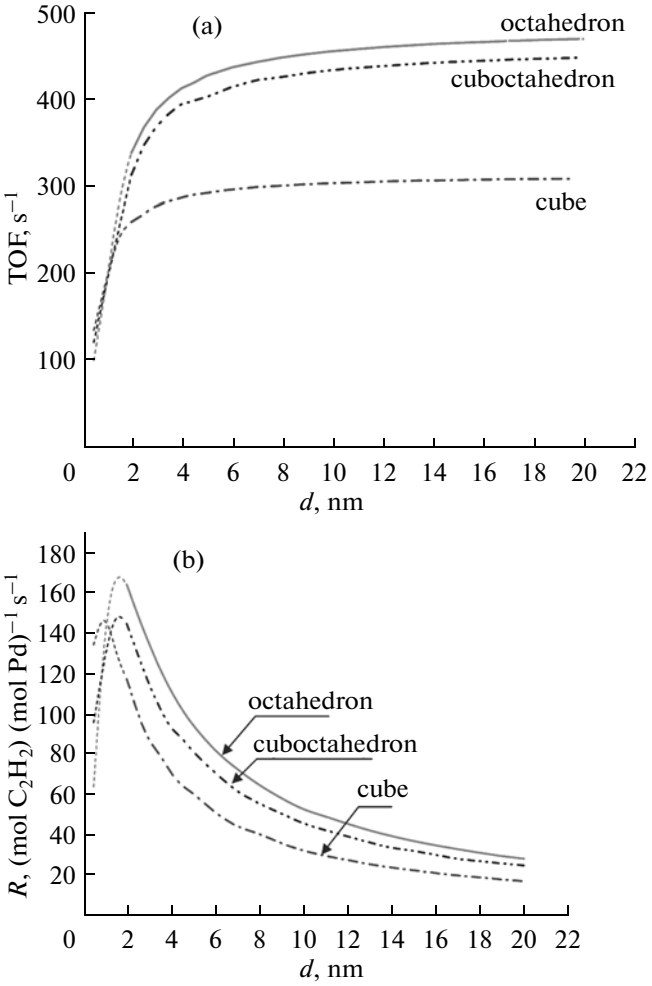

Fig. 6. Calculated optimization of the size and shape of nanoparticles based on data on (a) the catalyst turnover frequency and (b) reaction rate.

because the specific surface area of the catalyst decreases. Therefore, the optimum size of the particles should be determined for the achievement of maximum activity. The statistical approach [6] made it possible to calculate the catalyst turnover frequency and the reaction rate on palladium of cubic, cuboctahedral, and octahedral shapes over a wide range of particle sizes. Figure 6 shows the results. As can be seen, the results of the calculations coincide with the experimental data, confirming that the octahedral particles, which contain (111) faces, possess the greatest activity. The influence of particle size on the catalyst turnover frequency manifests itself in a range of 2–10 nm; then, the effect is almost imperceptible (Fig. 6a). Particles smaller than 2 nm lose their metallic properties [4]; therefore, their behavior cannot correspond to the model accepted. Figure 6 shows this region with dashed lines. However, if activity is expressed as the rate of acetylene conversion on a total Pd basis, the size effect is manifested more noticeably (Fig. 6b). In this case, octahedrons also exhibit the greatest activity. Particles of size about 2 nm exhibit a maximum; then, the activity decreases. The dependence on the particle size almost disappears when the size becomes greater than 20 nm.

Hence, the octahedral nanoparticles of size ~3 nm exhibit the greatest activity.

Thus, in this work, we used a colloidal method to obtain the nanoparticles of palladium of a cubic shape, which contain only (100) faces, octahedrons, which consist of only (111) faces, and cuboctahedrons with faces of both types. The PVP stabilizer was removed from the catalyst surface using the UV–O_3 method. Catalysts with various shapes of palladium nanoparticles were used in the reaction of selective acetylene hydrogenation for studying its structure sensitivity. Approximately the same selectivity was observed for all of the catalysts, and octahedral Pd particles containing (111) faces exhibited maximum activity. According to the model accepted, the reaction occurs at the surface atoms of all types. Nevertheless, the atoms located on the edges of the particles are less active than the atoms located on faces by one order of magnitude. In turn, atoms on the (111) face are more active than those on the (100) face by a factor of about 1.5. The proportions of atoms of different types depends on the size of the particle, and the type of the face depends on the shape of the particle. Thus, we demonstrated that both the size and the shape of the nanoparticles affect the catalyst activity. The octahedral Pd nanoparticles of size ~3 nm possess the highest activity.

REFERENCES

1. Mei, D., Shet, P.A., Neurock, M., and Smith, C.M., *J. Catal.*, 2006, vol. 242, no. 1, p. 1.
2. Borodzinski, A. and Cybulski, A., *Appl. Catal., A*, 2000, vol. 198, nos. 1–2, p. 51.
3. Molero, H., Bartlett, B.F., and Tysoe, W.T., *J. Catal.,* 1999, vol. 181, no. 1, p. 49.
4. Che, M. and Bennett, C.O., *Adv. Catal.,* 1989, vol. 36, p. 55.
5. Aduriz, H.R., Bodnariuk, P., Dennehy, M., and Gigola, C.E., *Appl. Catal.*, 1990, vol. 58, no. 2, p. 227.
6. Van Hardeveld, R. and Hartog, F., *Surf. Sci.,* 1969, vol. 15, no. 2, p. 189.
7. Molnar, A., Sarkany, A., and Varga, M., *J. Mol. Catal. A: Chem.*, 2001, vol. 173, nos. 1–2, p. 185.
8. Ruta, M., Semagina, N., and Kiwi-Minsker, L., *J. Phys. Chem. C*, 2008, vol. 112, no. 35, p. 13635.
9. Tribolet, P. and Kiwi-Minsker, L., *Catal. Today*, 2005, vol. 105, nos. 3–4, p. 337.
10. Binder, A., Seipenbusch, M., Muhler, M., and Kasper, G., *J. Catal.*, 2009, vol. 268, no. 1, p. 150.
11. Tao, A.R., Habas, S., and Yang, P.D., *Small*, 2008, vol. 4, no. 3, p. 310.
12. Xia, Y., Xiong, Y.J., Lim, B., and Skrabala, S.E., *Angew. Chem. Int. Ed.*, 2009, vol. 48, no. 1, p. 60.

13. Lange, C., De Caro, D., Gamez, A., Storck, S., Bradley, J.S., and Maier, W.F., *Langmuir*, 1999, vol. 15, no. 16, p. 5333.

14. Yu, R., Song, H., Zhang, X.F., and Yang, P.D., *J. Phys. Chem. B*, 2005, vol. 109, no. 15, p. 6940.

15. Lee, I., Morales, R., Albiter, M.A., and Zaera, F., *Proc. Natl. Acad. Sci. U.S.A.*, 2008, vol. 105, no. 40, p. 15241.

16. Vig, J.R., *J. Vac. Sci. Technol., A*, 1985, vol. 3, no. 3, p. 1027.

17. Aliaga, C., Park, J.Y., Yamada, Y., Lee, H.S., Tsung, C.K., Yang, P.D., and Somorjai, G.A., *J. Phys. Chem., C*, 2009, vol. 113, no. 15, p. 6150.

18. Pang, S.F., Kurosawa, Y., Kondo, T., and Kawai, T., *Chem. Lett.*, 2005, vol. 34, no. 4, p. 544.

19. Ruta, M., *PhD Thesis*, École Polytechnique Fédérale de Lausanne, 2008.

20. Tribolet, P. and Kiwi-Minsker, L., *Catal. Today*, 2005, vol. 102, no. 1, p. 15.

21. Lim, B., Jiang, M.J., Tao, J., Camargo, P.H.C., Zhu, Y.M., and Xia, Y.N., *Adv. Funct. Mater.,* 2009, vol. 19, no. 2, p. 189.

22. Mei, D.H., Neurock, M., and Smith, C.M., *J. Catal.*, 2009, vol. 268, no. 2, p. 181.

23. Coq, B. and Figueras, F., *J Mol. Catal. A: Chem.*, 2001, vol. 173, nos. 1–2, p. 117.

24. Bos, A.N.R. and Westerterp, K.R., *Chem. Eng. Process.*, 1993, vol. 32, no. 1, p. 1.

25. Borodzinski, A. and Golebiowski, A., *Langmuir*, 1997, vol. 13, no. 5, p. 883.